Arabian Journal of Chemistry (2023) **16**, 104698

King Saud University

Arabian Journal of Chemistry

www.ksu.edu.sa
www.sciencedirect.com

ORIGINAL ARTICLE

Electro-magnetic radiative flowing of Williamson-dusty nanofluid along elongating sheet: Nanotechnology application

Imran Ullah [a], Farhad Ali [b], Sharena Mohamad Isa [c], Saqib Murtaza [b], Wasim Jamshed [d,*], Mohamed R. Eid [e,f], Ayesha Amjad [g,h], Kamel Guedri [i], Hamiden Abd El-Wahed Khalifa [j,k], Sayed M El Din [l]

[a] *College of Civil Engineering, National University of Sciences and Technology, Islamabad 44000, Pakistan*
[b] *Department of Mathematics, City University of Information Technology, Peshawar 25000, Pakistan*
[c] *Universiti Kuala Lumpur Kampus Cawangan Malaysia Italy Design Institute, Malaysia*
[d] *Department of Mathematics, Capital University of Science and Technology (CUST), Islamabad 44000, Pakistan*
[e] *Department of Mathematics, Faculty of Science, New Valley University, Al-Kharga, Al-Wadi Al-Gadid, 72511, Egypt*
[f] *Department of Mathematics, Faculty of Science, Northern Border University, Arar 1321, Saudi Arabia*
[g] *Faculty of Organization & Management, Silesian University of Technology, 44-100 Gliwice, Poland*
[h] *Centre for Mechanical Engineering, Materials and Processes (CEMMPRE) University of Coimbra, Polo II, Coimbra, 3030-788, Portugal*
[i] *Mechanical Engineering Department, College of Engineering and Islamic Architecture, Umm Al-Qura University, P. O. Box 5555, Makkah 21955, Saudi Arabia*
[j] *Department of Mathematics, College of Science and Arts, Qassim University, Al-Badaya 51951,Saudi Arabia*
[k] *Department of Operations and Management Research, Faculty of Graduate Studies for Statistical Research, Cairo University, Giza 12613, Egypt*
[l] *Center of Research, Faculty of Engineering, Future University in Egypt, New Cairo 11835, Egypt*

Received 16 November 2022; accepted 19 February 2023
Available online 23 February 2023

KEYWORDS

Williamson Dusty fluid;
Nanofluidics;
MHD;
Mixed convection;

Abstract The flowing of nanomolecules in Williamson nanoliquids via a stretched sheet has a significant influence, and its demand in the manufacturing, therapeutic disciplines, medication, and cooking supplies is enormous and frequently reported. However, 2-dimensional (2-D) combined convective flowing of Williamson-dusty nanofluid (WDNF) via a stretchable sheet in the presence of a magneto force and the porous medium remains unidentified. Hence, this report inspects the

* Corresponding author.
E-mail address: wasiktk@hotmail.com (W. Jamshed).
Peer review under responsibility of King Saud University.

Production and hosting by Elsevier

https://doi.org/10.1016/j.arabjc.2023.104698

Nomenclature:

A	reference temperature
A^*	reference Concentration
B_0	strength of magnetic field ($kgs^{-2}A^{-1}$)
C_w	fluid Concentration at wall
C_∞	ambient concentration
C_{f_x}	skin friction coefficient
c_f	specific heat of fluid ($J/(K.kg)$)
c_n	specific heat of nanoparticles
c_p	specific heat of dust particles
D_B	Brownian diffusion coefficient
D_T	thermophoretic diffusion coefficient
Ec	Eckert number
G_r, G_r^*	Grashof numbers
g	gravitational force due to acceleration
K	porosity parameter
k_1	porousness of penetrable material
k_f	thermal conductance ($W/m.K$)
k_1^*	mean absorption coefficient
L_e	Lewis number
l	mass concentration of dust particles
M	magnetic parameter
N	buoyancy forces ratio
N_t	thermophoretic variant
N_b	Brownian factor
N_{u_x}	local Nusselt quantity
P_r	Prandtl quantity
q_r	radioactive heat fluxing
q_w	wall heat fluxing
q_s	wall mass fluxing
R	chemically reactive variant
R_d	radiative variant
Re_x	Reynolds quantity
Sh_x	local Sherwood quantity
T_f	convective liquid temperature
T	temperature
T_∞	ambient temperature
u, v	rapidity elements (m/s)
u_w	stretchable sheet speed (m/s)
W_e	Weissenberg number
x, y	coordinate axes

Greek letters

α_f	thermal diffusion
β_T	volumetric thermal expansion
β_1	momentum dust parameter
β_2	fluid interaction parameter
δ	specific heat ratio
η	similarity variable
ε	heat generation parameter
Γ	relaxation time
λ	combined convective variant
μ_f	liquid dynamical viscidness (kg/ms^3)
ν	kinematic viscosity (m^2/s)
ρ_f	fluid Density (kg/m^3)
ρ_p	density of dust phase
ϕ	dimensionless nanoparticle size
ψ	streaming function
σ	electric conductance
σ^*	Stefan Boltzmann value
τ	heat capacitance ratio
τ_m	recreation time of dusty molecules
τ_T	thermal balance time
τ_w	surface shearing stress
θ	nondimensional temperature

Subscripts

∞	constraint at ambient
w	constraint at surface

Thermal radiation; Nanomaterials

combined influence of Brownian and thermophoretic diffusion preserved in magneto WDNF modeling in the occurrence of radiative flowing. The Runge-Kutta Fehlberg approach (RKFA) is used to numerically study the problem of an ordinary differential system employing shooting techniques. The table also addresses the frictional force factor, heat, and mass transmission rate, as well as validates the current findings with earlier available results in the scheduled manner. The acquired outcomes demonstrate that a larger magnetic field decreases the rapidity and thickening of the impetus boundary layer of nanofluids. The momentum dust parameter and the fluid interaction parameter are shown to enhance the heat transmission rate. The rapidity and temperature fields of the liquid and dusty phases improved as the radiation parameter was raised on the contrary of magnetism force which causes dwindling in two phases. Consequently, the examined model's heat transference is reduced in the opposite direction of the Weissenberg number by the magnetic force. Additionally, it is found that higher thermophoresis parameters show an increasing trend in temperature for both phases.

1. Introduction

Nanofluid is the next-generation fluid that contains the predominant thermo-physical properties which empower it valuable in heat transport applications, including fusion power engines, cooling systems, heat exchangers, underground water cable systems, and many chemical processes (Esfe et al., 2014; Mashayekhi et al., 2018; Bazdar et al., 2020; Hassan et al., 2022). The new progressions in nanotechnology prompt the creation of a new group of liquids with advanced heat transport characteristics. Now the question comes to mind what is nanofluid? Nanofluid is the uniform and homogeneous combination of nanometer-scale-sized solid particles (oxide, silica, polymers, metals, non-metals, and carbon nanotubes) and conventional fluids (water, oils, alcohols, etc.) (Al-Kouz et al., 2021). In order to create improved heat transfer fluids with much greater thermal conductivities from an energy-saving and environmental cleansing point of view, a noble and novel technique that calls for the mixing of nanoparticles and the base fluid was devised. Nanoparticles possess high thermo-physical assets as linked to conventional liquids that accordingly upgrade the thermal transportation characteristics of the standard liquid. In 1995, the idea of suspension of nanoparticles was firstly coined by Choi and Eastman (Choi and Eastman, 1995) to root out the issues of Maxwell's work (Maxwell, 1873). The size range of nanoparticles is limited to 0 to 0.04 vol fraction because if the size of the nanoparticles surpasses this limit, sedimentation and clogging difficulties would occur. It is essential to specify here that nanofluids are not made by just embedding the nanoparticles in the base fluid but involve a specific chemical procedure to develop a homogenous mixture with effective and stable applications. Due to their potential implementation in the motion of dust-ladder air, fluid motion, gas-cooling strategies to improve heat transport, environmental degradation, powder innovation, geothermal power, nuclear reactor refrigeration, dust compendium, soil erosion, solid propellant nozzles, fossil fuel industry, crude oil sanitization, and so on, analyses of two-phase flowing in which solid sphere-shaped molecules are dispersed in base fluids are of great interest. Various specialists engaged in these technologies have worked on researching the momentum and heat transmission properties of a dusty liquid.

In laboratories, there are two techniques for preparing nanofluid: a one-step approach and a two-step method. In the scientific field, the two-step process for preparing nanofluid is commonly used. In the two steps method, primarily the raw material is converted to powder form through the physical or chemical procedure. Secondly, the powder is mixed with the regular fluid with highly extreme magnetic force, ultrasonic agitation, or homogenizing (Mukherjee and Paria, 2013). Nanofluid has improved characteristics such as increased heat capacitance, enhanced viscosity, higher thermal conductive, and advanced thermal transmit rate as linked to the conventional liquid. Using different nanofluids, Kavusi and Toghraie (Kavusi and Toghraie, 2017) created a two-dimensional numerical model to replicate the operation of a heat pipe. Through the use of the finite volume approach, the impact of various nanofluids at various concentrations and particle sizes on the functionality of heat pipes were also investigated. These important characteristics led Toghraie et al. (Toghraie et al., 2020) to examine the impact of heat fluxing profile in a concentric annulus utilizing H_2O-Al_2O_3 nanoliquid. By taking into account the radiative impact using single- and two-phase techniques with defined wall temperature circumstances and prescribed surface heat fluxing parameters, Mostafazadeh et al. (Mostafazadeh et al., 2019) analyzed heat transference and laminar flowing of a nanoliquid in a vertical pipe. Li et al. (Li et al., 2019) explored a non-Newtonian nanoliquid's two-phase mixed convection in a porousness h-shaped hole. They took four revolving cylinders and used the Boussinesq approximation to produce mixed convective within the enclosure. Najafabadi et al. (Najafabadi et al., 2022) discussed the mixed convection flow of nanofluid through a vertical channel. In another paper, Sarkar and Das (Sarkar and Das, 2022) discussed the heat transfer in a Cross nanofluid through a horizontal cylinder in the existence of magnetism force and chemical reaction. Ali et al. (Ali et al., 2022) reported the impact of Arrhenius activation energy in the electrical conductance flowing of nano liquid over a stretching cylinder. Some other important regarding applications of nanofluids can be seen in (Das et al., 2021; Ali et al., 2021; Ali et al., 2023; Jamshed et al., 2021; Najafabadi et al., 2022; Zangooee et al., 2022).

Dust granules and base fluid are combined to create the dusty fluid. As it has numerous uses in industry, engineering, and the field of medicine, including power technology, cooling nuclear reactors, recovering crude oil, the sedimentation process, treating wastewater, the formation of raindrops, environmental pollution, fluid-particle suspension past an elongated surface has received a great deal of research attention. In a variety of technological fields, the study of dusty fluids is of tremendous interest. Fluidization (flow of fluid through packed beds), flow in rocket tubes (when the metallic and carbon fuel particle is present together), the coalescing of small droplets (the process of formation of raindrops), extraction of matter from the fluid through a centrifugal separator, polymerization, fluid droplets sprays, purification of crude oil and cooling system are the areas having great technical importance. A noteworthy investigation of the complex plasma has been done by Fortov et al. (Fortov et al., 2005). They have reviewed the main types of experimental complex plasma, and many elementary operations, like the charging of grain in various regimes, the influence of change particles upon each other, and the exchange of momentum of various species are investigated. Time-dependent electro-hydrodynamic flowing of a dusty liquid flowing on a stretchable plate has been discussed by Ramesh et al. (Ramesh et al., 2012). The authors also took the cause of non-uniformly heat generating in their analysis. In alkaline anion exchange membranes, Grew et al. (Grew and Chiu, 2010) employed the dusty fluid model to predict hydroxyl anion thermal conduction study. Dusty fluid flow with time-dependent viscosity and conductivity between two parallel plates has been inspected by Makinde and Chinyoka (Makinde and Chinyoka, 2010). 2-D hybrid dusty fluid flow through non-Darcian material under the effect of Cattaneo-Christov thermal fluxing has been assessed by Reddy et al. (Reddy et al., 2020). Some other exciting and significant industrial applications of dusty fluid flow and thermal radiation influence can be seen in (Radhika et al., 2020; Kaneez et al., 2020; Ahmadi et al., 2020; Dadsetani et al., 2020; Safaei et al., 2020; Abuldrazzaq et al., 2020; Abu-Hamdeh et al., 2021; Khosravi et al., 2021; Safaei et al., 2021; Reddy and Ferdows, 2021).

The flowing and thermal exchange of a power-law liquid over a stretchable plate is an impressive standard problematic in rheology, with many implementations in a variety of manufacturing fields; instances incorporate chemical manufacturing polymer fluids, the coolant of an endless metal surface in a freezing immersion, crystal growing, hot rolling, exotic lubricants, and suspension solutions (Megahed, 2012; Gulzar et al., 2020; Attar et al., 2022; Faghiri et al., 2022; Alali and Megahed, 2022). Non-Newtonian materials play a significant role in many mechanical and chemical processes as well as engineering implementations. These compounds have an important use in medications, surfactants, petroleum engineering, blood, and numerous other areas. Williamson fluid, which is a type of pseudoplastic fluid, is one of the non-Newtonian fluids. Williamson originally created the Williamson liquid in his pioneering study on pseudo-plastic materials flow. He developed a modeling approach to explain the flowing of shear-thinning liquids and tested this theory with experimentation. Several more investigators have applied the Williamson liquid since then. Keeping in view the characteristics of Williamson fluid, Hashim et al. (Hashim and Khan, 2018) probed the time-dependent combined convective flowing of Williamson nanofluid. The authors considered variable conductivity and magnetic field in their study. Impact of dual chemically reactive flowing along with the influence of active energy on Williamson nanoliquid has been evaluated by Hamid et al. (Hamid and Khan, 2018). In another paper, Hamid et al (Hamid et al., 2018) investigated the stagnating point flowing of Williamson liquid created by stretchable plate together with the impact of Ohmic heat. The phenomenon of thermal radiation and viscous dissipation in Wil-

liamson liquid flowing generated results in the stretchable wall has been reported by Megahed (Megahed, 2019). Reddy et al. (Reddy et al., 2022) discussed quantitatively the thermal radiation implications of Williamson nanoliquid flow alongside a stretched plate with porosity media while accounting for velocity and thermal slippage via the Keller box method. Other concerned and significant work on Williamson nanofluid can be found in (Hamid et al., 2019; Hamid et al., 2019; Hamid et al., 2019).

We discovered that the mixed convection Williamson dusty nanoliquid flowing produced by a stretchy plate in a porousness medium has never been investigated before. To close this gap, research is done on the 2-D mixed convection flowing of Williamson dusty nanofluid on a stretchy plate in the existence of a cross-cut magnetism force and radiative flowing. The goal of the current problem is to analyze the impact of thermal radiative fluxing on the electrical conductance flowing of Williamson's dusty nanofluid through a porous medium. The controlling PDEs are converted to non-linear ODEs using suitable similarity transform variables and then solved numerically. Plots are generated and thoroughly analyzed to provide insight into the ramifications of entered dimensionless parameters.

2. Mathematical formulation

Consider combined convective flowing of WDNF initiated by stretchable plate. The surface is expanded with the rapidity of $u_w(x) = ax$, wherein a is constant. The $x-$ axis is measured via the surface axis, whereas the $y-$ axis is measured in the path of flowing (Fig. 1(a)).

In the present problem, we made the following assumptions.

1. In the perpendicular direction, a transverse magnetic field of intensity B_0 is applied.
2. It is presumed that the plate's surface is warmed by the temperature $T_w(x) = T_\infty + Ax$ in which A being reference temperature and concentration is $C_w(x) = C_\infty + A^* x$, where A^* shows the source concentricity.
3. The temperature and concentricity at the ambient are T_∞ and C_∞, correspondingly.
4. The nanofluid is non-Newtonian, laminar, electrically conducting, and incompressible.
5. For steady laminar flow, the Boussinesq approximation is used.

The principal equalities for impetus, energy, and mass along with the continuity equation are given as (Ramesh et al., 2012; Makinde and Chinyoka, 2010; Kaneez et al., 2020):

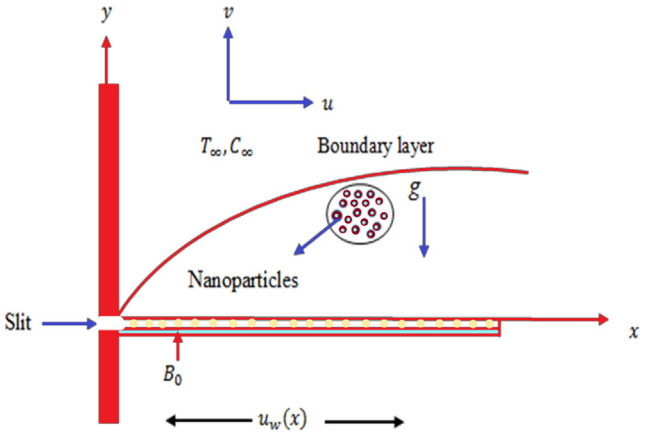

Fig. 1a Physical model and Coordinate system.

2.1. For fluid Phase:

$$\frac{\partial u}{\partial x} + \frac{\partial v}{\partial y} = 0 \tag{1}$$

$$u\frac{\partial u}{\partial x} + v\frac{\partial u}{\partial y} = \frac{\mu}{\rho_f}\frac{\partial^2 u}{\partial y^2} + \sqrt{2}\Gamma\frac{\partial u}{\partial y}\frac{\partial^2 u}{\partial y^2} - \frac{\sigma B_0^2}{\rho_f}u - \frac{\mu}{\rho_f k_1}u + \frac{\rho_p}{\rho_f \tau_m}(u_p - u) + \left[(1 - C_\infty)\frac{\rho_{f_\infty}}{\rho_f}\beta_T(T - T_\infty) - \frac{\left(\rho_n - \rho_{f_\infty}\right)}{\rho_f}(C - C_\infty)\right]g \tag{2}$$

$$u\frac{\partial T}{\partial x} + v\frac{\partial T}{\partial y} = \alpha_f\frac{\partial^2 T}{\partial y^2} + \tau\left[D_B\frac{\partial C}{\partial y}\frac{\partial T}{\partial y} + \frac{D_T}{T_\infty}\left(\frac{\partial T}{\partial y}\right)^2\right] - \frac{1}{(\rho c)_n}\frac{\partial q_r}{\partial y} - \frac{\rho_p c_p}{\tau_T}(T_p - T) + \frac{\rho_p c_p}{\tau_m}(u_p - u)^2 \tag{3}$$

$$u\frac{\partial C}{\partial x} + v\frac{\partial C}{\partial y} = D_B\frac{\partial^2 C}{\partial y^2} + \frac{D_T}{T_\infty}\frac{\partial^2 T}{\partial y^2} \tag{4}$$

2.2. For dust phase:

$$\frac{\partial u_p}{\partial x} + \frac{\partial v_p}{\partial y} = 0 \tag{5}$$

$$u_p\frac{\partial u_p}{\partial x} + v_p\frac{\partial v_p}{\partial y} = \frac{\rho_p}{\tau_m}(u - u_p), \tag{6}$$

$$u_p\frac{\partial T_p}{\partial x} + v_p\frac{\partial T_p}{\partial y} = -\frac{c_p}{c_m\tau_T}(T_p - T) \tag{7}$$

In the previous equations, u and v labeled the quickness elements in x and y trends correspondingly, μ is dynamic viscidness, Γ is the relaxation time, ρ_f is the fluid consistency, ρ_p is the consistency of the dust phase, ρ_n is the consistency of nanoliquid, g is the gravitational force due to acceleration, k_1 is the porousness of the penetrable material, τ_m is the relaxation time of dusty molecules, β_T is the thermal expansion amount, $\alpha_f = \frac{k}{(\rho c)_f}$ signifies the thermal diffusion of a liquid, k denotes the thermal conductance, $\tau = \frac{(\rho c)_n}{(\rho c)_f}$ signifies the relative amount of heat capacitances wherein $(\rho c)_f$ symbols of the liquid heat capacitance and $(\rho c)_n$ signifies the nanomolecules heat capacitance, D_B signifies the Brownian motion factor, D_T denotes the thermophoretic variable, q_r symbols of the radiation heat fluxing, τ_T implies the thermal balance time and c_m signifies the specific heat of dusty particles.

The subsequent bounder constraints are created as next (Megahed, 2012)

$$u = u_w, v = 0, T = T_w, T_p = T_w, C = C_w \text{ at } y = 0, \tag{8}$$

$$u \to 0,\ u_p \to 0, T \to T_\infty\ ,\ T_p \to 0, C \to C_\infty \text{ as } y \to \infty. \tag{9}$$

The Rosseland guesstimate is applied to represent the radioactive heat fluxing q_r in energy equality (Gulzar et al., 2020);

$$q_r = \frac{-4\sigma^*}{3k_1{}^*}\frac{\partial T^4}{\partial y}. \tag{10}$$

where σ^* symbols the Stefan Boltzmann value and $k_1{}^*$ is the mean absorbing amount. T^4 may be represented as a temperature-dependent linearly function. We dilate T^4 in a Taylor series about T_∞ and ignoring larger bounds, acquired

$$T^4 \cong 4T_\infty^3 T - 3T_\infty^4 \tag{11}$$

Now propose the streaming function ψ, a similarity parameter η, and the similarity modifications shown below (Attar et al., 2022)

$$\left.\begin{aligned} u = axf'(\eta), v = -\sqrt{av}f(\eta), u_p = axF'(\eta), v_p = -\sqrt{av}F(\eta), \\ \theta(\eta) = \frac{T-T_\infty}{T_w-T_\infty}, \theta_p(\eta) = \frac{T_p-T_\infty}{T_w-T_\infty}, \phi(\eta) = \frac{C-C_\infty}{C_w-C_\infty}. \end{aligned}\right\} \tag{12}$$

By using the above transformations, the systematic of equalities (2–7) will get

$$f-+ff''-f'^2+Wef''f--(M+K)f\prime+l\beta_1(F\prime-f\prime) + \lambda(\theta+N\phi)=0 \tag{13}$$

$$FF''-F'^2+l\beta_1(F'-f')=0 \tag{14}$$

$$\frac{1}{\Pr}\left(1+\frac{4}{3}R_d\right)\theta''+f\theta\prime+N_b\phi'\theta\prime+N_t\theta'^2 l\beta_2(\theta_p-\theta) + l\beta_1 Ec(F\prime-f\prime)^2=0, \tag{15}$$

$$\theta_p'F-\delta\beta_2(\theta_p-\theta)=0 \tag{16}$$

$$\frac{1}{Le}\phi\prime\prime+f\phi'+\frac{N_t}{N_b}\theta\prime\prime=0 \tag{17}$$

The associated bounder constraints conditions are given as

$$f(0)=0, f'(0)=1,\ \theta(0)=1, \phi(0)=1, \tag{18}$$

$$f'(\infty)=0,\ F(\infty)\to 0, \theta(\infty)=0, \theta_p(\infty)=0,\ \phi(\infty)=0 \tag{19}$$

Where We, M, K, l, β_1, λ, N, β_2, Pr, R_d, N_t, N_b, Ec, Le, δ, Gr and Gr^* are the Weissenberg number, magnetic parameter, porosity constraint, mass concentricity of dusty molecules, momentum dusty variable, mixed convection factor, buoyancy forces ratio, fluid interaction constraint, Prandtl amount, radiative variable, thermophoresis parameter, Brownian diffusion factor, Eckert quantity, Lewis amount, specific heat ratio and Grashof numbers, and are defined as

$$\left.\begin{aligned} We=\Gamma x\sqrt{\frac{2a^3}{v}}, M=\frac{\sigma B_0^2}{a\rho_f}, K=\frac{v}{k_1}, l=\frac{\rho_p}{\rho_f}, \beta_1=\frac{1}{\tau_m a}, \\ \lambda=\frac{Gr}{Re_x^2}, N=\frac{(\rho_p-\rho_{f\infty})(C_w-C_\infty)}{(1-C_\infty)\rho_{f_\infty}\beta_T(T_w-T_\infty)}, \beta_2=\frac{1}{\tau_T a}, Pr=\frac{v}{\alpha_f}, \\ R_d=\frac{4\sigma^* T_\infty^3}{kk_1{}^*}, N_t=\frac{\tau D_T(T_w-T_\infty)}{v}, N_b=\frac{\tau D_B(C_w-C_\infty)}{v}, \\ Ec=\frac{u_w{}^2}{c_f(T_w-T_\infty)}, Le=\frac{v}{D_B}, \delta=\frac{c_p}{c_m}, \\ Gr=\frac{(1-C_\infty)\left(\frac{\rho_{f\infty}}{\rho_f}\right)g\beta_T(T_w-T_\infty)x^3}{v^2}, Gr^*=\frac{\left(\frac{(\rho_p-\rho_{f\infty})}{\rho_f}\right)g(C_w-C_\infty)x^3}{v^2} \end{aligned}\right\} \tag{20}$$

The surface drag force, surface heat fluxing, and wall mass fluxing, separately, are described as

$$\tau_w=\mu\left[\frac{\partial u}{\partial y}+\frac{\Gamma}{\sqrt{2}}\left(\frac{\partial u}{\partial y}\right)^2\right]_{y=0},$$
$$q_w=-\left[\left(\alpha_f+\frac{16\sigma^* T_\infty^3}{3\rho c_p k_1^*}\right)\frac{\partial T}{\partial y}\right]_{y=0}, q_s=-D_B\left(\frac{\partial C}{\partial y}\right)_{y=0} \tag{21}$$

The non-dimensional skin friction coefficient $C_{f_x}=\frac{\tau_w}{\rho_f u_w^2}$, the local Nusselt number $Nu_x=\frac{xq_w}{\alpha_f(T_w-T_\infty)}$ and local Sherwood number $Sh_x=\frac{xq_s}{D_B(C_w-C_\infty)}$ on the sheet alongside x- orientation, local Nusselt quantity Nu_x and Sherwood quantity Sh_x are provided as

$$(Re_x)^{\frac{1}{2}}Cf_x=2\left[f\prime\prime(0)+\frac{We}{2}f''^2(0)\right],$$
$$(Re_x)^{-\frac{1}{2}}Nu_x=-\left(1+\frac{4}{3}R_d\right)\theta'(0),$$
$$(Re)^{-1/2}Sh_x=-\phi'(0) \tag{22}$$

where $Re_x=\frac{ax^2}{v}$ is the Reynold quantity.

3. Results and discussion

The 4th order Runge-Kutta based shooting procedure is used to solve the coupled ordinary differential Eqs. (13–17) concerning the boundary conditions (18) and (19) (Fig. 1(b)).

For computational outcomes, we considered $0 \le We \le 0.4$, $0 \le M \le 1.5$, $0 \le K \le 1.5$, $0 \le \beta_1 \le 1.5$, $1 \le \lambda \le 4$, $0 \le \beta_2 \le 1.5$, $0.72 \le Pr \le 7$, $0 \le R_d \le 3$, $0.4 \le N_b \le 1$, $0.4 \le N_t \le 1$. Except for the varying values indicated in the individual figures, these values are kept consistent throughout the study. Table 1 and Table 2 show a comparison of the skin friction coefficient and the Nusselt number, respectively, which were found to be in excellent agreement.

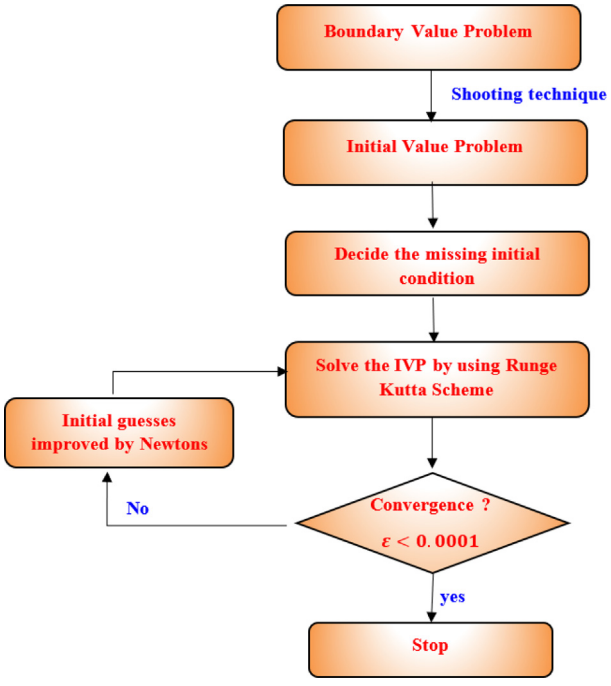

Fig. 1b Flow Chart of 4th order Runge Kutta with shooting procedure.

Table 1 Comparison of frictional force factor for various amounts of M at $We = 0$.

f″ (0)			
M	Ref. (Akbar et al., 2013)	Ref. (Ali, 2006)	Present results
1	−1.41421	−1.41421	−1.41421
5	−2.44948	−2.44948	−2.44949
10	−3.31662	−3.31662	−3.31662
50	−7.14142	−7.14142	−7.14141
500	–22.3830	–22.3830	–22.38301
1000	−31.6386	−31.6386	−31.63857

Table 2 Comparison of Nusselt quantity for several amounts of Pr in the absence of nanoparticles at $M = 0, R_d = 0$ and $Ec = 0$.

$-\theta'(0)$			
Pr	Ref. (Ali, 2006)	Ref. (Chen, 1998)	Present results
1	−0.5801	−0.58199	−0.58222
3	−1.1599	−1.16523	−1.16522
5	–	–	−1.56802
10	−2.2960	−2.30796	−2.30797
100	–	–	−7.76562

Moreover, Table 3 demonstrates the influence of different factors on the frictional force coefficient, Nusselt, and Sherwood numbers.

Figs. 2(a) and 2(b) depict the influence of We on quickness and energy profiles in both liquid and dust phases. The Weissenberg quantity is a measurable relationship between the fluid's recreation and a particular procedure time. The mounting values of the Weissenberg number cause an upsurge in the recreation on time of liquid molecules, which causes the viscosity to be more important and produces an impedance to a liquid flowing, resulting in a dwindle in liquid speed. The rapidity

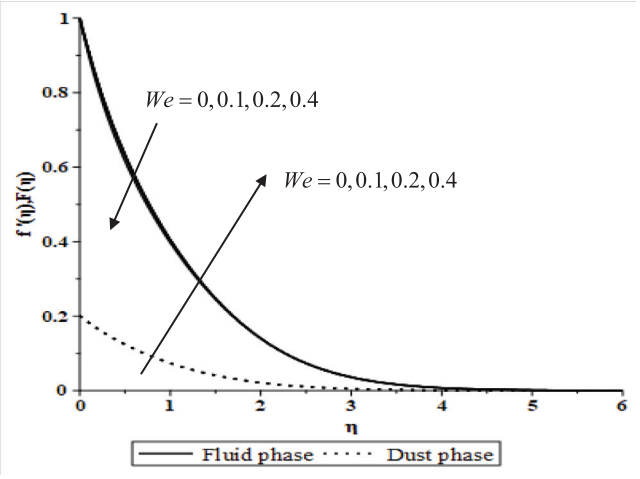

Fig. 2a Variation of $f'(\eta)$ and $F(\eta)$ for We.

outline and related boundary layer thickening for the liquid phase reduce and the dust phase increases as the We grows, however temperature boundary layer thickening increases for liquid and dust phases as We increases.

Figs. 3(a) and 3(b) demonstrate how the magnetic parameter affects the velocity and temperature profiles in together liquid and dusty phases. The graphs show that increasing the magnetic parameter diminishes the velocity field whilst increasing temperature outlines for together liquid and dusty phases. Because of the Lorentz force, which is the polar opposite of the flow when the magnetic field parameter is increased, which in turn upsurges the energy stored inside the fluid molecules and thus rises the temperature. This force tends to diminish the thickener of the quickness bounder-layer while growing the thickener of the thermal bounder-layer. As a result, the temperature profiles of a flow have risen. A similar effect is noticed for the variation of porosity parameter K with rapidity and energy fields for together liquid and dusty phases, as

Table 3 Influence of diverse factors on drag force coefficient, Nusselt numbers, and Sherwood numbers. Fixed parameter: $Pr = 7, l = 0.5, N = 1, Ec = 0.01$ and $R_d = 1$.

We	β_1	β_2	N_b	N_t	M	$(Re_x)^{1/2}Cf_x$	$(Re_x)^{-1/2}Nu_x$	$(Re_x)^{-1/2}Sh_x$
0	0.5	0.5	0.5	0.5	1	−0.954866	−0.647637	−0.628831
0.1						−0.979693	−0.646592	−0.622475
0.3						−1.046023	−0.642499	−0.625030
0.1	0.0	0.5	0.5	0.5	1	−0.906574	−0.654557	−0.638399
	0.5					−0.979693	−0.646592	−0.622475
	1.0					−1.027364	−0.640390	−0.619932
0.1	0.5	0.0	0.5	0.5	1	−1.013378	−0.396491	−2.471301
		0.5				−0.979693	−0.646592	−0.622475
		1.0				−0.963116	−0.791605	−0.504067
0.1	0.5	0.5	0.4	0.5	1	−0.900352	−0.822992	−1.570139
			0.8			−1.092792	−0.317124	−2.811889
			1.0			−1.125097	−0.200458	−3.089430
0.1	0.5	0.5	0.5	0.4	1	−1.027824	−0.627917	−1.132522
				0.8		−0.8658207	−0.665138	−0.978264
				1.0		−0.809900	−0.654170	−1.877018
0.1	0.5	0.5	0.5	0.5	0	−0.600820	−0.647875	−1.044207
					0.5	−0.796787	−0.647773	−0.818533
					1.0	−0.979693	−0.646592	−0.622475

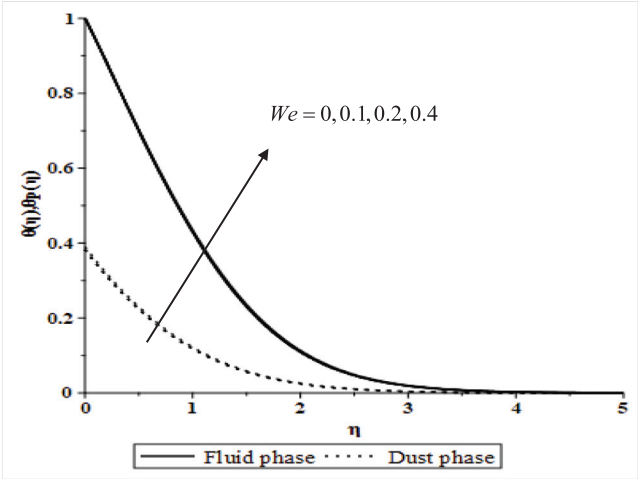

Fig. 2b Variation of $\theta(\eta)$and $\theta_p(\eta)$ for We.

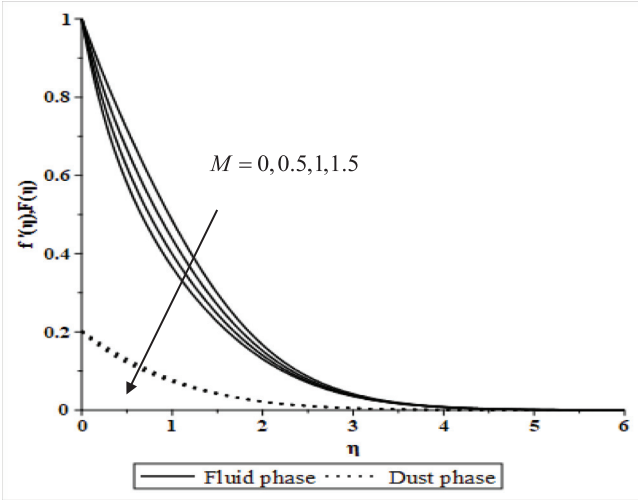

Fig. 3a Variation of $f'(\eta)$ and $F(\eta)$ for M.

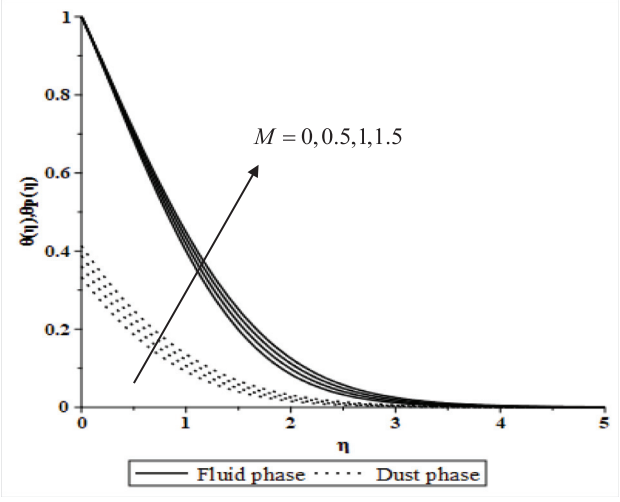

Fig. 3b Variation of $\theta(\eta)$and $\theta_p(\eta)$ for M.

shown in Figs. 4(a) and 4(b). This behavior is explained physically by the porous medium's inertial imparting resistance to the fluid flow mechanisms, causing the fluid to travel at a slower rate and at a lower velocity. Furthermore, as the number of dusty molecules in a liquid rose, a drag force increased, creating more impedance to a liquid flowing and, eventually, a reduction in the quickness field and a growth in an energy field. This effect is due to the physical explanation which considers the augmented pores to be the reason behind this.

Figs. 5(a) and 5(b) portray the impact of momentum dust variable on quickness and energy outlines for liquid and dusty phases. It's worth noting that when β_1 increases, the rapidity of a liquid phase decreases while the speed of a dusty phase increases, as illustrated in Fig. 5(a). Since the fluid-particle phase contact is so strong, the particle phase exerts an opposing force on a liquid phase up to the molecule's rapidity and approaches a liquid swiftness. Increasing the β_1 value improves the temperature outline of the liquid and dusty stages, as shown in Fig. 5(b). This is consistent with the common fact that contact among a liquid and molecules stages improves flow thermal conductance. Furthermore, an increase in β_1

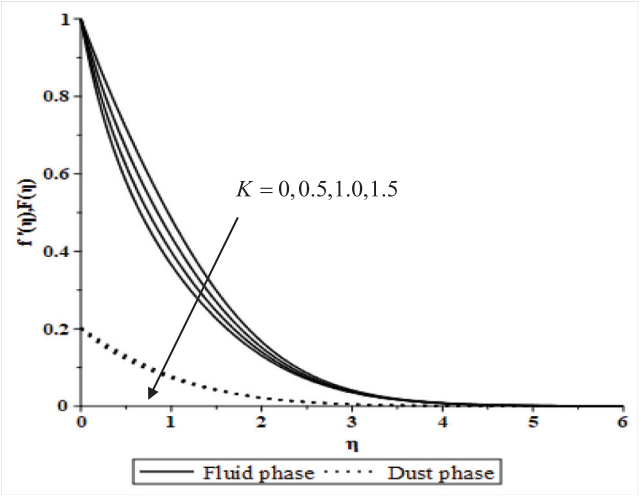

Fig. 4a Variation of $f'(\eta)$ and $F(\eta)$ for K.

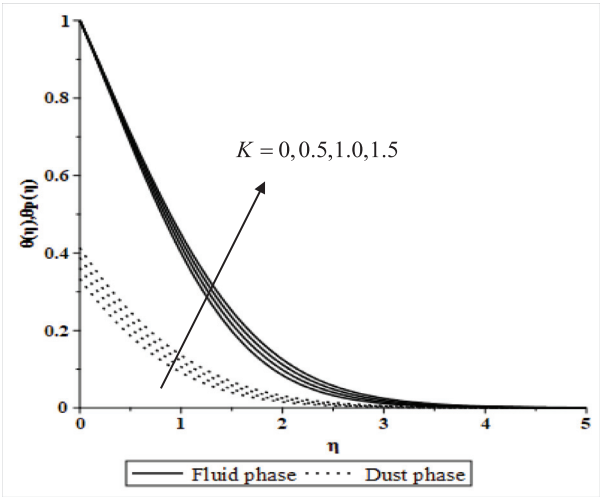

Fig. 4b Variation of $\theta(\eta)$and $\theta_p(\eta)$ for K.

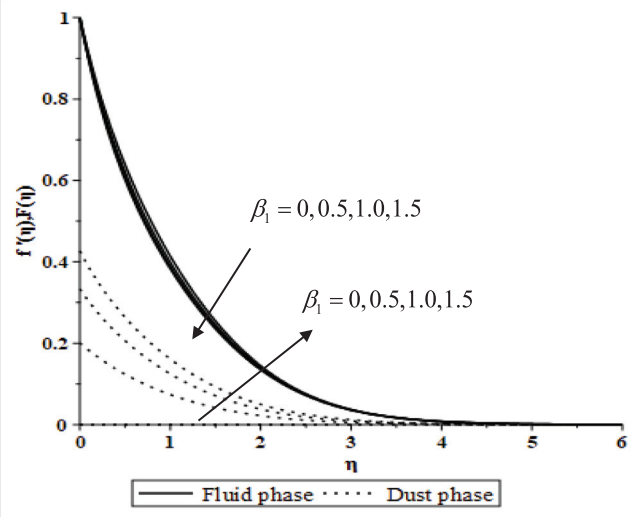

Fig. 5a Variation of $f'(\eta)$ and $F(\eta)$ for β_1.

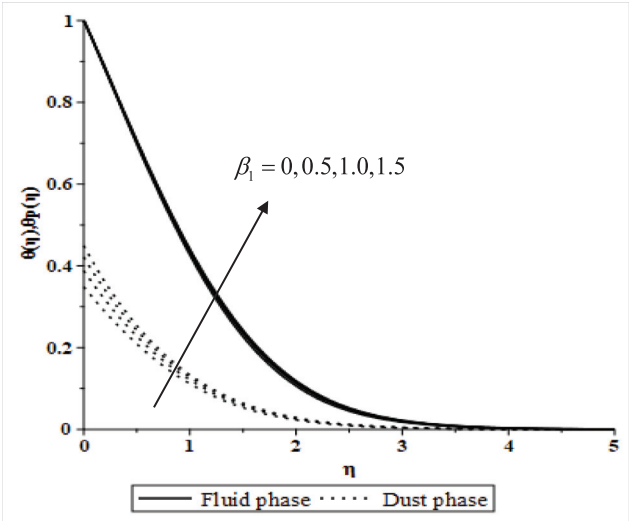

Fig. 5b Variation of $\theta(\eta)$and $\theta_p(\eta)$ for β_1.

causes the internal opponent power to the flowing to developing until the rapidity of a nanofluid phase is reached by the dust phase.

Figs. 6(a) and 6(b) illustrate the variation of λ on rapidity and energy outlines of liquid and dusty stages. It has been observed that the liquid and dusty stage velocities boosted with growth λ and the liquid and dusty phase temperatures decreased. Because of greater λ, buoyancy force takes precedence over viscous force. Following this, the buoyancy force parameter improves liquid flowing, which manages to boost fluid velocity and the corresponding boundary layer thickening. Further, this might happen when high buoyant values obtained enable the liquid to waste thermal and kinetic energy from dusty particle collisions, leading both numbers to drop at the top edge. Moreover, the mixed convection parameters combine the flow and heat fields. This represents the ability of the liquid to expand thermally. This is the underlying concept of liquid-in-glass thermometers. A rise in temperature causes the liquid to expand, causing it to ascend the glass.

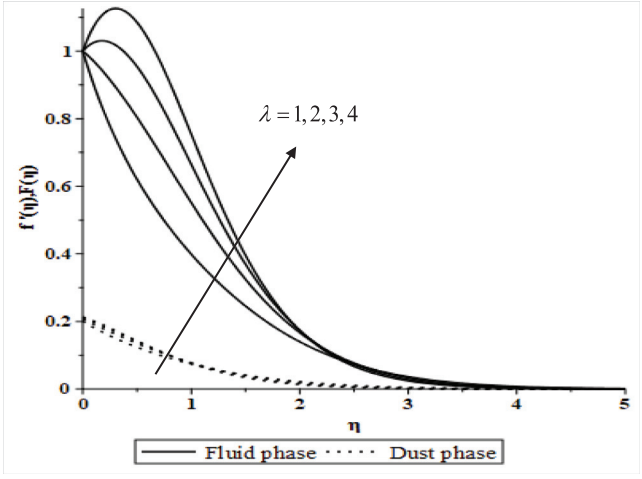

Fig. 6a Variations of $f'(\eta)$ and $F(\eta)$ for λ.

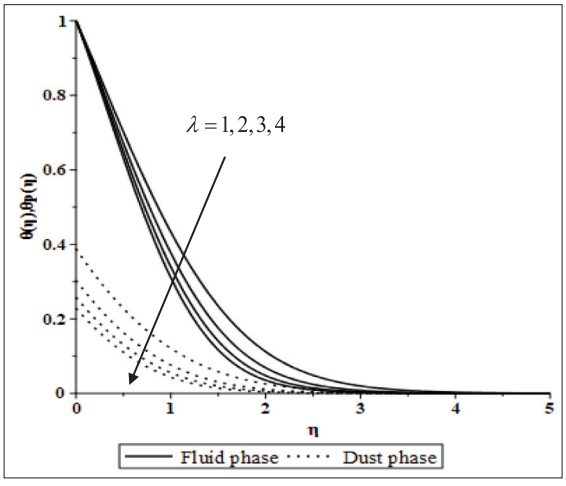

Fig. 6b Variations of $\theta(\eta)\theta_p(\eta)$ for λ.

Figs. 7(a) and 7(b) exhibit the effect of β_2 on the rapidity and temperature outlines for together liquid and dusty phases. Fig. 7(a) shows that as β_2 value increases, the rapidity of the fluid and dusty phases decline. On the other hand, the temperature of the fluid phase tends to decrease as the β_2 increases and the temperature of the dusty phase rise as demonstrated in Fig. 7(b). Result the dusty elements generate frictional force in the liquid, slowing it down. This might be owing to enhanced contact between the nanoparticle phase and the dust particle phase, which allows for more conduction heat transfer in the dusty phase. Also, up until the dust phase reaches the fluid phase's rapidity, the fluid phase and flow are opposed internally as the liquid particles interface parameter increases. Moreover, this may happen because the liquid and particle phases interact strongly, leading to the particle phase developing an opposing force to the liquid phase until the particle speed reaches the liquid rapidity. Figs. 8(a) and 8(b) show the effect of *Pr* on the rapidity and temperature outlines of both the liquid and dust phases. The relationship between momentum and thermal conductivity is expressed in Prandtl number. The increase in *Pr* has a greater effect on the decrease in thermal bounder-layer thickener than on the impetus

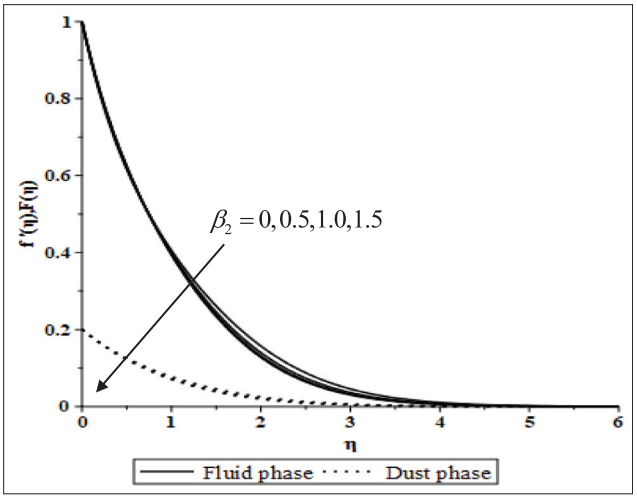

Fig. 7a Variations of $f'(\eta)$ and $F(\eta)$ for β_2.

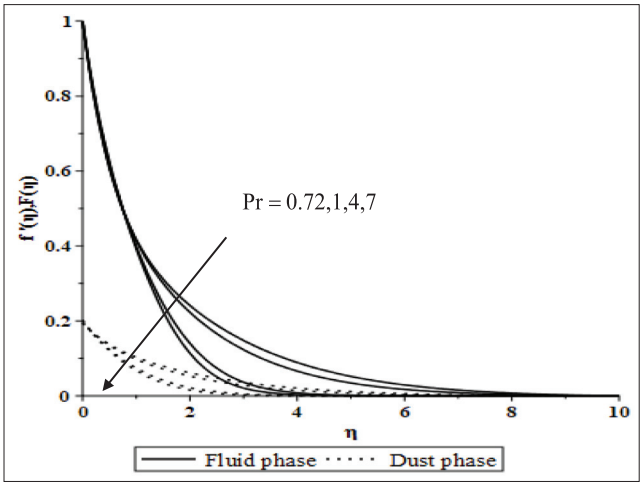

Fig. 8a Variation of $f'(\eta)$ and $F(\eta)$ for Pr.

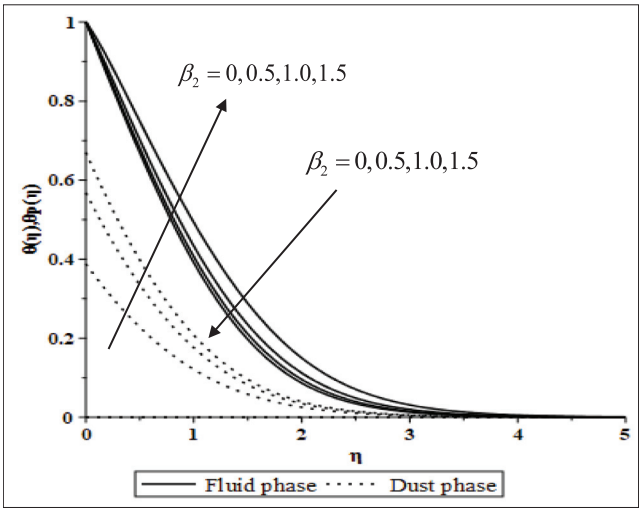

Fig. 7b Variation of $\theta(\eta)$and $\theta_p(\eta)$ for β_2.

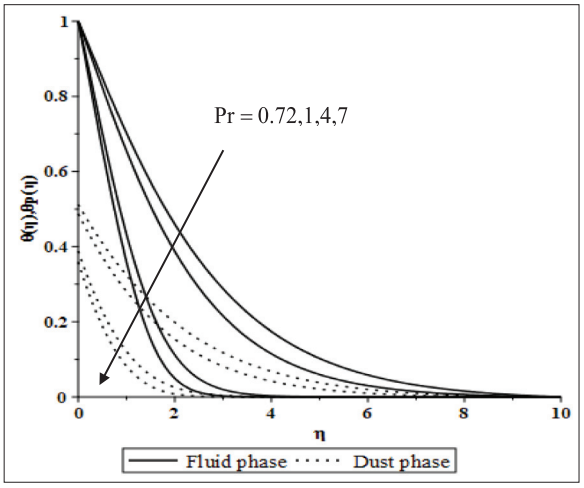

Fig. 8b Variation of $\theta(\eta)$and $\theta_p(\eta)$ for Pr.

bounder-layer thickener. In a heat transport situation, the Prandtl number is utilized to govern the relative impetus and thickening of the temperature bounder-layer. The rate of thermal diffusivity slows as Pr rises, resulting in a decline in thermal bounder- layer thickener. Physically, the fluid with a lesser Prandtl quantity has greater thermal conductance and a bigger thermal bounder-layer structure, allowing heat to permeate from the plate more quickly than the liquid with a greater Prandtl quantity, which has a thinner boundary layer.

Figs. 9(a) and 9(b) are plotted to visualize the appearance of R_d on quickness and temperature outlines of liquid and dusty phases. Interestingly, the quickness and energy fields of both liquid and dusty stages rise with growing amounts of R_d. The following behaviour can be explained physically by the fact that large warming rates of solely viscous nanofluids can also be predicted using the thermal radiation phenomenon. Another possible reason could be because the Stefan–Boltzmann value dominates, and the mean absorbing factor has less influence in the Rosseland approximation. Also, higher radiation parameter values increase the heating of the fluid, improv-

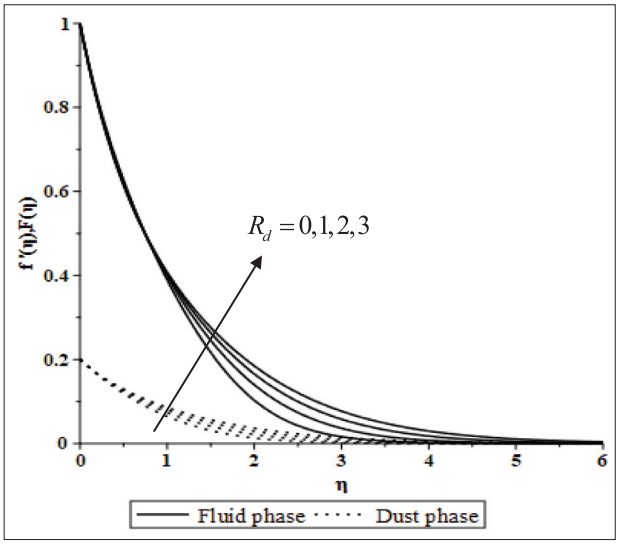

Fig. 9a Variation of $f'(\eta)$ and $F(\eta)$ for R_d.

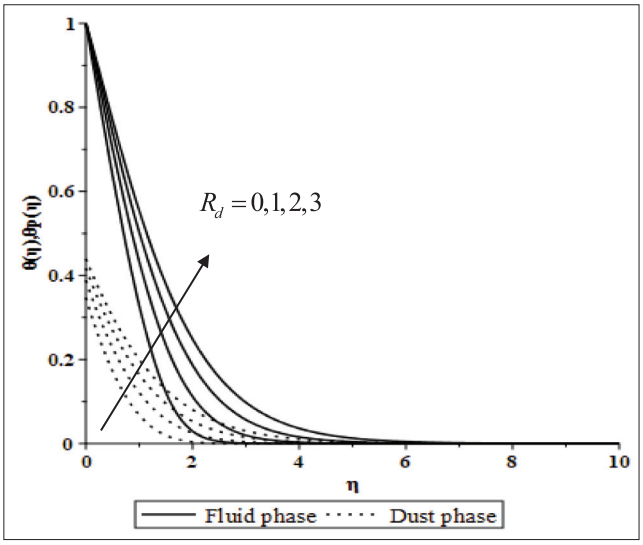

Fig. 9b Variations of $\theta(\eta)$and $\theta_p(\eta)$ for R_d.

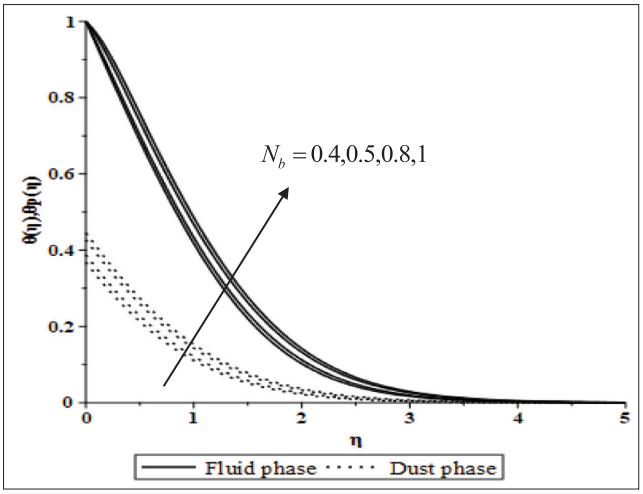

Fig. 10b Variation of $\theta(\eta)$and $\theta_p(\eta)$ for N_b.

ing the energy outline and the thickener of the thermal bounder-layer between the liquid and dusty stages. Radiation enhances a conductive effect and tends to expand the thermal bounder-layer. This will improve the rapidity and temperature at any point away from the sheet metal surface. The excess radiation upsurges the turbulence of the fluid particles' movement, including dust particles as well, which surges internal collisions and increases the stored energy, raising the fluid's velocity and improving temperatures.

Figs. 10(a) and 10(b) elucidate the variation of N_b on rapidity and temperature of the liquid and dusty phases. It can be seen that rapidity and temperature outlines for both liquid and dusty phases enhance with increasing values of N_b. A high Brownian motion parameter value represents that nanoparticles and base fluid particles collide frequently. As a result, there is an enhancement in heat transference qualities within the system, resulting in enhanced temperature and velocity fields. Figs. 11(a) and 11(b) describe the variation of rapidity and temperature profiles for increasing values of N_t for

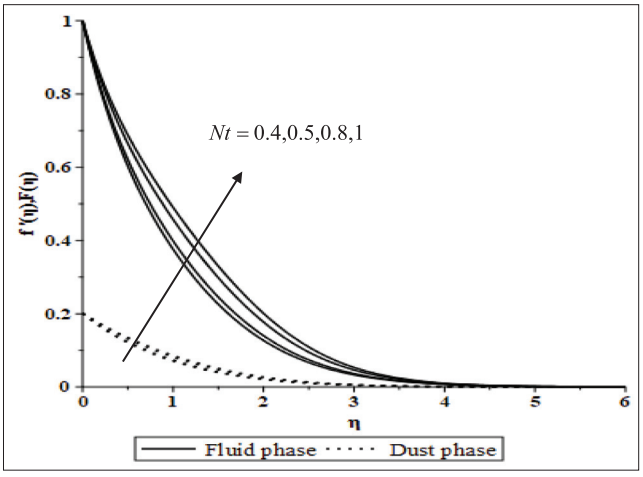

Fig. 11a Variation of $f'(\eta)$ and $F(\eta)$ for N_t.

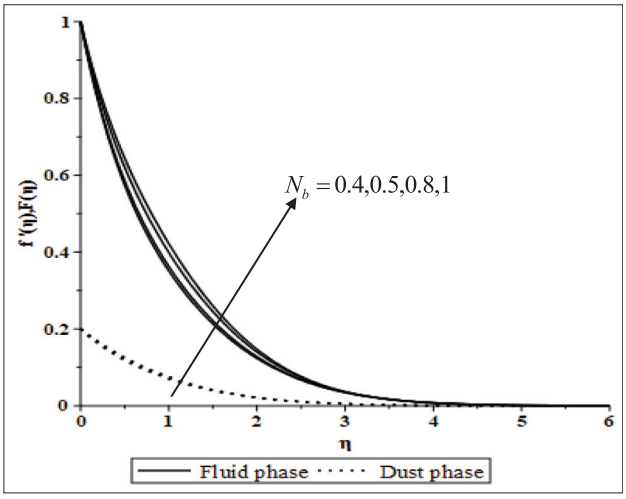

Fig. 10a Variations of $f'(\eta)$ and $F(\eta)$ for N_b.

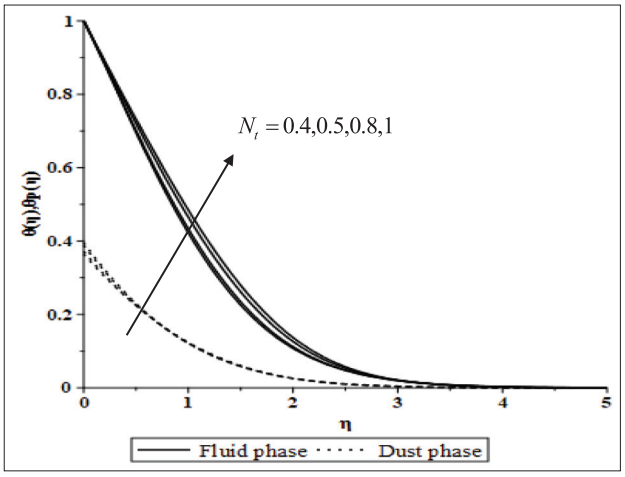

Fig. 11b Variation of $\theta(\eta)$and $\theta_p(\eta)$ for N_t.

together liquid and dusty phases. The thermophoretic force between the particles grows as the temperature difference in the system increases, causing the dusty nanofluid to heat up and the temperature of the nanofluid and dusty nanofluid to rise. Furthermore, this force can move suspended particles from a warm to a cold state, boosting the nanoparticle's strength in the fluid.

4. Conclusion

The flowing of a Williamson-dusty nanoliquid across a stretched plate has been studied using magnetohydrodynamic (MHD) mixed convection. The similarity solutions are achieved by applying the Runge Kutta Fehlberg technique and Maple software's algebraic code. The following are significant findings:

- The increment in We diminishes the velocity of the nanofluid while the dusty phase improved.
- The temperature of both the nanoliquid and the dusty phase are enlarged with the upsurge in We.
- A rise in M increased the fluid temperature while decreasing the fluid velocity.
- The influence of K on the temperature field of the dust phase is more profound than the rapidity of the dusty phase.
- The improvement of β_1 cause an augmentation in the quickness and energy of the dust phase.
- β_2 has an opposing influence on the temperature field of both fluid and dust phases.
- Increasing λ has a significant impact on the temperature field of both phases.
- Velocity and thermal fields show the same behavior of an improvement with the growing amounts of R_d.
- An expansion in the N_t leads to a growth in both the temperature and velocity of both phases.
- Higher values of β_1 and β_2 were shown to cause a drop in the heat transfer coefficient.

In the future, the existing method might be used to a number of physical and technical obstacles (Jamshed and Aziz, 2018; Jamshed, 2021; Jamshed and Nisar, 2021; Jamshed et al., 2021; Jamshed, 2021; Jamshed et al., 2022; Islam et al., 2022; Pasha et al., 2022; Rasool et al., 2022; Rasool et al., 2022; Rasool et al., 2022).

CRediT authorship contribution statement

Imran Ullah: Conceptualization. **Farhad Ali:** Formal analysis. **Sharena Mohamad Isa:** Methodology. **Saqib Murtaza:** Software. **Wasim Jamshed:** Validation, Investigation. **Mohamed R. Eid:** Investigation, Validation, Writing - original draft, Writing - review & editing. **Ayesha Amjad:** Writing – review & editing.

Declaration of Competing Interest

The authors declare that they have no known competing financial interests or personal relationships that could have appeared to influence the work reported in this paper.

Acknowledgment

The researchers would like to thank the Deanship of Scientific Research, Qassim University for funding the publication of this project.

References

Abu-Hamdeh, N.H., Alsulami, R.A., Rawa, M.J., Aljinaidi, A.A., Alazwari, M.A., Eltaher, M.A., Almitani, K.H., Alnefaie, K.A., Abusorrah, A.M., Sindi, H.F., Goodarzi, M., Safaei, M.R., 2021. A detailed hydrothermal investigation of a helical micro double-tube heat exchanger for a wide range of helix pitch length. Case Stud. Therm. Eng. 28, 101413.

Abuldrazzaq, T., Togan, H., Alsulami, H., Goodarzi, M., Safaei, M. R., 2020. Heat transfer improvement in a double backward-facing expanding channel using different working Fluids. Symmetry. 12 (7), 1088.

Ahmadi, A.A., Arabbeiki, M., Ali, H.M., Goodarzi, M., Safaei, M.R., 2020. Configuration and optimization of a minichannel using water–alumina nanofluid by non-dominated sorting genetic algorithm and response surface method. Nanomaterials 10 (5), 901.

Akbar, N.S., Nadeem, S., Haq, R.U., Khan, Z.H., 2013. Numerical solutions of Magnetohydrodynamic boundary layer flow of tangent hyperbolic fluid towards a stretching sheet. Indian J Phys. 87 (11), 1121–1124.

Alali, E., Megahed, A.M., 2022. MHD dissipative Casson nanofluid liquid film flow due to an unsteady stretching sheet with radiation influence and slip velocity phenomenon. Nanotechnol. Rev. 11 (1), 463–472.

Ali, M.E., 2006. The effect of variable viscosity on mixed convection heat transfer along a vertical moving surface. Int J Therm Sci. 45 (1), 60–69.

Ali, A., Sarkar, S., Das, S., Jana, R.N., 2021. Investigation of cattaneo–christov double diffusions theory in bioconvective slip flow of radiated magneto-cross-nanomaterial over stretching cylinder/plate with activation energy. Int. J. Appl. Comput. Math 7 (5), 208.

Ali, A., Sarkar, S., Das, S., Jana, R.N., 2022. A report on entropy generation and Arrhenius kinetics in magneto-bioconvective flow of Cross nanofluid over a cylinder with wall slip. Int. J. Amb. Ener. 15, 1–6.

Ali, A., Sarkar, S., Das, S., 2023. Bioconvective chemically reactive entropy optimized Cross-nano-material conveying oxytactic microorganisms over a flexible cylinder with Lorentz force and Arrhenius kinetics. Math. Comput. Simul. 205, 1029–1051.

Al-Kouz, W., Bendrer, B.A.I., Aissa, A., Almuhtady, A., Jamshed, W., Nisar, K.S., et al, 2021. Galerkin finite element analysis of magneto two-phase nanofluid flowing in double wavy enclosure comprehending an adiabatic rotating cylinder. Sci. Rep. 11 (1), 1–15.

Attar, M.A., Roshani, M., Hosseinzadeh, K., Ganji, D.D., 2022. Analytical solution of fractional differential equations by Akbari–Ganji's method. Partial Differ. Equations Appl. Math. 6, 100450.

Bazdar, H., Toghraie, D., Pourfattah, F., Akbari, O.A., Nguyen, H. M., Asadi, A., 2020. numerical investigation of turbulent flow and heat transfer of nanofluid inside a wavy microchannel with different wavelengths. J Therm Anal Calorim. 139 (3), 2365–2380.

Chen, C.-H., 1998. Laminar mixed convection adjacent to vertical, continuously stretching sheets. Heat Mass Transf. 33 (5–6), 471–476.

Choi, S. U. S., Eastman, J. A. 1995. Enhancing Thermal Conductivity of Fluids with Nanoparticles. Proc. 1995 ASME Int. Mech. Engineering Congr. Expo. SanFrancisco, USA, ASME, FED231/MD66 99–105.

Dadsetani, R., Sheikhzadeh, G.A., Safaei, M.R., Leon, A.S., Goodarzi, M., 2020. Cooling enhancement and stress reduction optimization of disk-shaped electronic components using nanofluids. Symmetry. 12 (6), 931.

Das, S., Ali, A., Jana, R.N., 2021. Darcy-Forchheimer flow of a magneto-radiated couple stress fluid over an inclined exponentially stretching surface with Ohmic dissipation. World J. Eng. 18 (2), 345–360.

Esfe, M.H., Akbari, M., Toghraie, D.S., Karimipour, A., Afrand, M., 2014. Effect of nanofluid variable properties on mixed convection flow and heat transfer in an inclined two-sided lid-driven cavity with sinusoidal heating on sidewalls. Heat Transfer Research. 45 (5), 409–432.

Faghiri, S., Akbari, S., Shafii, M.B., Hosseinzadeh, K., 2022. Hydrothermal analysis of non-Newtonian fluid flow (blood) through the circular tube under prescribed non-uniform wall heat flux *Theor*. Appl. Mech. Lett. 12, (4) 100360.

Fortov, V.E., Ivlev, A.V., Khrapak, S.A., Khrapak, A.G., Morfill, G. E., 2005. Complex (dusty) plasmas: Current status, open issues, perspectives. Phys. Rep. 421 (1–2), 1–103.

Grew, K.N., Chiu, W.K., 2010. A dusty fluid model for predicting hydroxyl anion conductivity in alkaline anion exchange membranes. J Electrochem Soc. 157 (3), B327.

Gulzar, M.M., Aslam, A., Waqas, M., Javed, M.A., Hosseinzadeh, K., 2020. A nonlinear mathematical analysis for magneto-hyperbolic-tangent liquid featuring simultaneous aspects of magnetic field, heat source and thermal stratification. Appl. Nanosci. 10, 4513–4518.

Hamid, A., Khan, M., Hafeez, A., 2018. Unsteady stagnation-point flow of Williamson fluid generated by stretching/shrinking sheet with Ohmic heating. Int J Heat Mass Transf. 126, 933–940.

Hamid, A., Khan, M., 2018. Impacts of binary chemical reaction with activation energy on unsteady flow of magneto-Williamson nanofluid. J. Mol. Liq. 262, 435–442.

Hamid, A., Alghamdi, M., Khan, M., Alshomrani, A.S., 2019. An investigation of thermal and solutal stratification effects on mixed convection flow and heat transfer of Williamson nanofluid. J Mol Liq. 284, 307–315.

Hamid, A., Hafeez, A., Khan, M., Alshomrani, A.S., Alghamdi, M., 2019. Heat transport features of magnetic water–graphene oxide nanofluid flow with thermal radiation: Stability Test. Eur J Mech-B/Fluids. 76, 434–441.

Hamid, A., Khan, M., Alghamdi, M., 2019. Numerical simulation for transient flow of Williamson fluid with multiple slip model in the presence of chemically reacting species. Int J Numer Meth Heat Fluid Flow. 29 (11), 4445–4461.

Hashim, H.A., Khan, M., 2018. Unsteady mixed convective flow of Williamson nanofluid with heat transfer in the presence of variable thermal conductivity and magnetic field. J Mol Liq. 260, 436–446.

Hassan, M., Mebarek-Oudina, F., Faisal, A., Ghafar, A., Ismail, A.I., 2022. Thermal energy and mass transport of shear thinning fluid under effects of low to high shear rate viscosity. Int. J. Thermofluids. 15, 100176.

Islam, N., Pasha, A.A., Jamshed, W., Ibrahim, R.W., Alsulami, R., 2022. On Powell-Eyring hybridity nanofluidic flow based Carboxy-Methyl-Cellulose (CMC) with solar thermal radiation: A quadratic regression estimation. Int. Commun. Heat Mass Transfer 138, 106413.

Jamshed, W., 2021. Numerical Investigation of MHD Impact on Maxwell Nanofluid. Int. Commun. Heat Mass Transfer 120 (5), 683.

Jamshed, W., 2021. Finite element method in thermal characterization and streamline flow analysis of electromagnetic silver-magnesium oxide nanofluid inside grooved enclosure. Int. Commun. Heat Mass Transfer 130, 105795.

Jamshed, W., Aziz, A., 2018. Entropy Analysis of TiO_2-Cu/EG Casson Hybrid Nanofluid via Cattaneo-Christov Heat Flux Model. Applied Nanosciences 08, 01–14.

Jamshed, W., Eid, M.R., Aissa, A., Mourad, A., Nisar, K.S., Shahzad, F., Vijayakumar, V., 2021. Partial velocity slip effect on working magneto non-Newtonian nanofluids flow in solar collectors subject to change viscosity and thermal conductivity with temperature. PLoS One 16 (11), e0259881.

Jamshed, W., Eid, M.R., Al-Hossainy, A.F., Raizah, Z., Tag El Din, E.S.M., Sajid, T., 2022. Experimental and TDDFT materials simulation of thermal characteristics and entropy optimized of Williamson Cu-methanol and Al_2O_3-methanol nanofluid flowing through solar collector. Sci. Rep. 12, 18130.

Jamshed, W., Nisar, K.S., 2021. Computational single phase comparative study of Williamson nanofluid in parabolic trough solar collector via Keller box method. Int. J. Energy Res. 45 (7), 10696–10718.

Jamshed, W., Nisar b, K.S., Ibrahim, R.W., Shahzad, F., Eid, M.R., 2021. Thermal expansion optimization in solar aircraft using tangent hyperbolic hybrid nanofluid: a solar thermal application. J. Mater. Res. Technol. 14, 985–1006.

Kaneez, H., Nawaz, M., Alaoui, M.K., Abdelmalek, Z., 2020. An enhancement in transportation of heat energy in yield stress dusty fluid via mono and hybrid nanoparticles. Phys Scr. 95, (8) 085216.

Kavusi, H., Toghraie, D., 2017. A comprehensive study of the performance of a heat pipe by using of various nanofluids. Adv. Powder Technol. 28 (11), 3074–3084.

Khosravi, R., Rabiei, S., Khaki, M., Safaei, M.R., Goodarzi, M., 2021. Entropy generation of graphene–platinum hybrid nanofluid flow through a wavy cylindrical microchannel solar receiver by using neural networks. J. Therm. Anal. Calorim. 145, 1949–1967.

Li, Z., Barnoon, P., Toghraie, D., Dehkordi, R.B., Afrand, M., 2019. Mixed convection of non-Newtonian nanofluid in an H-shaped cavity with cooler and heater cylinders filled by a porous material: Two phase approach. Adv. Powder Technol. 30 (11), 2666–2685.

Makinde, O.D., Chinyoka, T., 2010. MHD transient flows and heat transfer of dusty fluid in a channel with variable physical properties and Navier slip condition. Comput Math Appl. 60 (3), 660–669.

Mashayekhi, R., Khodabandeh, E., Akbari, O.A., Toghraie, D., Bahiraei, M., Gholami, M., 2018. CFD analysis of thermal and hydrodynamic characteristics of hybrid nanofluid in a new designed sinusoidal double-layered microchannel heat sink. J. Therm. Anal. Calorim. 134 (3), 2305–2315.

Maxwell, J.C., 1873. In: A treatise on electricity and magnetism, Vol. 1. Clarendon Press, Oxford.

Megahed, A.M., 2012. Variable viscosity and slip velocity effects on the flow and heat transfer of a power-law fluid over a non-linearly stretching surface with heat flux and thermal radiation. Rheol Acta 51 (9), 841–847.

Megahed, A.M., 2019. Williamson fluid flow due to a nonlinearly stretching sheet with viscous dissipation and thermal radiation. J Egy Math Soc. 27 (1), 1–10.

Mostafazadeh, A., Toghraie, D., Mashayekhi, R., Akbari, O.A., 2019. Effect of radiation on laminar natural convection of nanofluid in a vertical channel with single- and two-phase approaches. J. Therm. Anal. Calorim. 138 (1), 779–794.

Mukherjee, S., Paria, S., 2013. Preparation and stability of nanofluids-a review. IOSR J Mech Civil Eng. 9 (2), 63–69.

Najafabadi, M.F., Rostami, H.T., Hosseinzadeh, K., Ganji, D.D., 2022. Hydrothermal study of nanofluid flow in channel by RBF method with exponential boundary conditions. Proc. Inst. Mech. Eng. Part E J. Process Mech. Eng. 09544089221133909.

Najafabadi, M.F., TalebiRostami, H., Hosseinzadeh, K., Ganji, D.D., 2022. Investigation of nanofluid flow in a vertical channel considering polynomial boundary conditions by Akbari-Ganji's method. Theor. Appl. Mech. Lett. 12, (4) 100356.

Pasha, A.A., Islam, N., Jamshed, W., Alam, M.I., Jameel, A.G.A., Juhany, K.A., Alsulami, R., 2022. Statistical analysis of viscous hybridized nanofluid flowing via Galerkin finite element technique. Int. Commun. Heat Mass Transfer 137, 106244.

Radhika, M., Sowmya, G., Prasannakumara, B.C., Alam, M., Rahimi-Gorji, M., Rahaman, M., 2020. The flow of fluid-particle suspension between two rotating stretchable disks with the effect of the external magnetic field. Phys Scr. 96, (1) 015214.

Ramesh, G.K., Gireesha, B.J., Bagewadi, C.S., 2012. MHD flow of a dusty fluid near the stagnation point over a permeable stretching sheet with non-uniform source/sink. Int J Heat Mass Transf. 55 (17–18), 4900–4907.

Rasool, G., Saeed, A.M., Lare, A.I., Abderrahmane, A., Guedri, K., Vaidya, H., Marzouki, R., 2022. Darcy-Forchheimer Flow of Water Conveying Multi-Walled Carbon Nanoparticles through a Vertical Cleveland Z-Staggered Cavity Subject to Entropy Generation. Micromachines 13, 744. https://doi.org/10.3390/mi13050744.

Rasool, G., Shafiq, A., Hussain, S., Zaydan, M., Wakif, A., Chamkha, A.J., Bhutta, M.S., 2022. Significance of Rosseland's Radiative Process on Reactive Maxwell Nanofluid Flows over an Isothermally Heated Stretching Sheet in the Presence of Darcy-Forchheimer and Lorentz Forces: Towards a New Perspective on Buongiorno's Model. Micromachines 13, 368. https://doi.org/10.3390/mi13030368.

Rasool, G., Shah, N.A., El-Zahar, E.R., Wakif, A., 2022. Numerical investigation of EMHD nanofluid flows over a convectively heated riga pattern positioned horizontally in a Darcy-Forchheimer porous medium: application of passive control strategy and generalized transfer laws. Waves Random Complex Media. https://doi.org/10.1080/17455030.2022.2074571.

Reddy, M.G., Ferdows, M., 2021. Species and thermal radiation on micropolar hydromagnetic dusty fluid flow across a paraboloid revolution. J Therm Anal Calorim. 143 (5), 3699–3717.

Reddy, Y.D., Mebarek-Oudina, F., Goud, B.S., Ismail, A.I., 2022. Radiation, velocity and thermal slips effect toward mhd boundary layer flow through heat and mass transport of Williamson nanofluid with porous medium. Arab. J. Sci. Eng. 21, 1–5.

Reddy, M.G., Rani, M.S., Kumar, K.G., Prasannakumar, B.C., Lokesh, H.J., 2020. Hybrid dusty fluid flow through a Cattaneo-Christov heat flux model. Physica A: Stat Mech Appl. 551, 123975.

Safaei, M.R., Tlili, I., Gholamalizadeh, E., Abbas, T., Alkanhal, T.A., Goodarzi, M., Dahari, M., 2020. Thermal analysis of a binary base fluid in pool boiling system of glycol–water alumina nanosuspension. J. Therm. Anal. Calorim. 143 (3), 2453–2462.

Safaei, M.R., Elkotb, A., Alsharif, A.M., Mansir, I.B., Alamri, S., Tirth, V., Goodarzi, M., 2021. An innovative design of a high strength and low weight sudden micro expansion by considering a nanofluid: Electronic cooling application. Case Stud. Therm. Eng. 28, 101637.

Sarkar, S., Das, S., 2022. Magneto-thermo-bioconvection of a chemically sensitive Cross nanofluid with an infusion of gyrotactic microorganisms over a lubricious cylindrical surface: Statistical analysis. Int. J. Model. Simul. 13, 1–22.

Toghraie, D., Mashayekhi, R., Arasteh, H., Sheykhi, S., Niknejadi, M., Chamkha, A.J., 2020. Two-phase investigation of water-Al2O3 nanofluid in a micro concentric annulus under non-uniform heat flux boundary conditions. Int. J. Numer. Methods Heat Fluid Flow. 30 (4), 1795–1814.

Zangooee, M.R., Hosseinzadeh, K., Ganji, D.D., 2022. Hydrothermal analysis of Hybrid nanofluid flow on a vertical plate by considering slip condition. Theor. Appl. Mech. Lett. 12, (5) 100357.